



This is the accepted manuscript made available via CHORUS. The article has been published as:

Saturation of Vortex Rings Ejected from Shock-Accelerated Interfaces

Michael J. Wadas, Loc H. Khieu, Griffin S. Cearley, Heath J. LeFevre, Carolyn C. Kuranz, and Eric Johnsen

Phys. Rev. Lett. **130**, 194001 — Published 12 May 2023

DOI: [10.1103/PhysRevLett.130.194001](https://doi.org/10.1103/PhysRevLett.130.194001)

Saturation of vortex rings ejected from shock-accelerated interfaces

Michael Wadas,^{1,*} Loc Khieu,¹ Griffin Cearley,¹ Heath LeFevre,¹ Carolyn Kuranz,¹ and Eric Johnsen¹

¹*University of Michigan, Ann Arbor, Michigan 48109*

Structures evoking vortex rings can be discerned in shock-accelerated flows ranging from astrophysics to inertial confinement fusion. By constructing an analogy between vortex rings produced in conventional propulsion systems and rings generated by a shock impinging upon a high-aspect-ratio protrusion along a material interface, we extend classical, constant-density vortex-ring theory to compressible multifluid flows. We further demonstrate saturation of such vortex rings as the protrusion aspect ratio is increased, thus explaining morphological differences observed in practice.

The mixing induced by the interaction of shocks with interfaces separating different fluids has implications for problems ranging from inertial confinement fusion (ICF) to astrophysics. In ICF, laser-generated shocks pass through layers of a capsule containing fusion fuel, compressing and heating it to extreme conditions at which self-sustained nuclear fusion may occur [1–4]. The mixing of the capsule material with fuel in the hotspot due to imperfections on the capsule surface and from the gas fill tube is a primary source of decreased performance [5–11]. In core-collapse supernovae, shocks generated from rapid energy release propagate outward through the layers of the collapsing stars, causing heavy core elements to jet into outer layers [12–16]. An understanding of these turbulent, shock-driven mixing phenomena is crucial for the success of ICF and may help elucidate the mechanisms by which heavy and light elements mix in the universe. While efforts are underway to develop models describing these turbulent phenomena [17, 18], their initialization is problematic given the lack of understanding of the transition to turbulence in these shock-accelerated flows.

As it traverses a perturbed material interface, a shock deposits baroclinic vorticity due to the misalignment of the density and pressure gradients, driving interfacial perturbation growth via the Richtmyer-Meshkov instability (RMI) [19, 20]. Perturbations initially grow linearly in time before saturating and rolling up into a mushroom-like shape as nonlinear effects dominate [21, 22]. Theoretical studies have long described early-time RMI dynamics in terms of point vortices or vortex sheets [23–26]. In complex situations (e.g., multimode, re-shock, late times, etc.), the multi-material mixing region may evolve to turbulence [27–31], which spreads as eddies entrain adjacent fluid parcels of different densities [32, 33]. Although linear and, to some extent, early nonlinear theory describing perturbation growth is well established [22, 34–36], turbulence transition and late-time mixing are poorly understood due to the inhomogeneity and intermittency of the flow. There is no doubt, however, that vorticity dynamics play a role in transition and mixing [26, 37, 38].

Advances in diagnostics, in particular, micron-scale x-ray imaging with Fresnel zone plates and lithium fluoride detector [39–42], and numerical methods have enabled

high-resolution visualizations of shock-induced mixing regions. In recent studies [10, 29, 43–49], flow structures intermittently ejected from the mixing region can be discerned, in some cases to distances many times their characteristic length, as illustrated in Figure 1. Though explicitly connected to vortex rings [30, 48, 50, 51], these structures cannot be described by (nonlinear) RMI theory or existing models [34, 35, 47, 52–54]. A criterion for vortex dipole ejection based on the initial interface geometry was developed [47], though this study fell short of quantitatively describing the ejection mechanism. Predicting this shock-induced ejection of vortex rings is critical to determine the growth of the mixing region because these structures transport kinetic energy and circulation from the mixing region and therefore affect its size and intensity. Furthermore, such rings may perturb other flow structures away from the mixing region (e.g., other nearby interfaces). While vortex rings generated by drawing a piston in an open-ended cylinder have received significant attention in a completely different context [55, 56], the mechanism explaining the formation and ejection of vortex rings and dipoles from shock-induced mixing regions has yet to be established.

In this letter, we outline a theory quantitatively describing the formation, ejection, and evolution of vortex rings from shock-accelerated interfaces. Drawing from classical studies [55], we develop a setup enabling us to

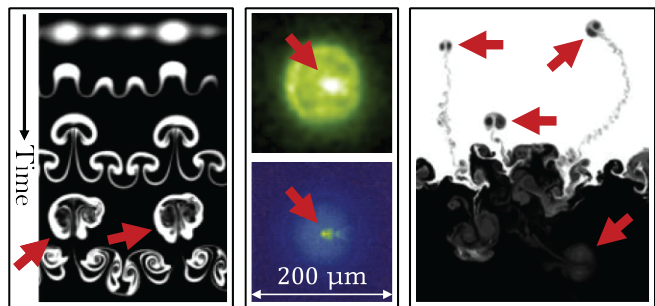


FIG. 1. Left: evolution of a multimode shocked fluid layer experiment (Taylor & Francis Ltd www.tandfonline.com) [44]. Middle: experimental (top) and simulated (bottom) x-ray self-emission during an ICF capsule implosion [45]. Right: volume fraction from RMI simulations [43]. Red arrows indicate likely vortex rings/dipoles. All images are reproduced with permission.

* mwadas@umich.edu

systematically investigate the formation and ejection of vortex rings from mixing regions generated by the interaction of a shock with an interface. Our analysis, verified by direct simulations of the Euler equations, fully describes the vortex ring dynamics, thereby extending classical theory for piston/cylinder systems to more general geometries and vorticity sources, including compressible multifluid flows. This theory allows us to calculate the kinetic energy and circulation leaving the confines of the mixing region, which are key quantities in turbulence modeling, and identify situations when vortex ring saturation occurs. Furthermore, our theory may elucidate flows dominated by shock-induced jets at interfaces, such as those observed in ICF due to the fill tube and capsule defects [10, 45, 46], astrophysics [16, 57–59], and possibly ejecta physics [60, 61].

We first revisit the basic attributes of classical vortex rings in propulsion systems, in which an impulsively started jet is generated by forcing a piston through a hollow cylinder. The vortex sheet produced along the inner edge of the orifice separates and rolls up to form a ring [62–64]. As long as the ring is attached to the jet, it accumulates circulation as it convects downstream. However, beyond a critical stroke-to-diameter ratio, the ring detaches from the jet, and no additional circulation can be imparted to it. Over a wide range of experiments and simulations [65–71], this saturation occurs at a stroke-to-diameter ratio of approximately 4, deemed the *formation number*, which equivalently represents the timescale over which vortex rings form by expressing the stroke length as the time-integrated piston velocity [55, 56].

Given morphological similarities between classical vortex rings and rings ejected from shock-accelerated interfaces (see supplemental material [72]), we postulate that the vorticity deposited by a shock interacting with a high-aspect-ratio protrusion along a material interface serves the same purpose as that produced along the cylinder wall. If this hypothesis is correct, vortex rings ejected from shock-accelerated interfaces would exhibit behavior similar to classical rings, e.g., in terms of their circulation and formation number (including saturation), as well as their energy and impulse. We therefore expect that an initial interfacial geometry analogous to the cylinder may lead to similar vorticity dynamics. As illustrated in Figure 2, we set up our problem with heavy fluid of density ρ_H adjacent to light fluid of density ρ_L , with a heavy-fluid protrusion of diameter D and depth L in the light fluid. The shock propagates from right to left. The compression ratio across the shock $\rho_{H'}/\rho_H$ characterizes the shock strength (equivalently, a Mach number, M , could be defined), where $\rho_{H'}$ is the density of the shocked heavy fluid. The shock is transmitted through the interface, compressing the light fluid to density ρ_{L^*} , and a rarefaction is reflected from the interface, decompressing the shocked heavy fluid to density ρ_{H^*} . These densities are obtained by solving the Riemann problem initialized between the unshocked light fluid and the shocked heavy fluid. The protrusion, modelled as decompressed shocked

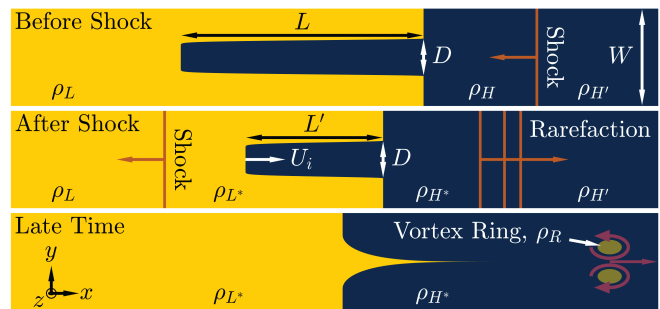


FIG. 2. Schematic showing the problem setup. Top: a shock approaches an interface separating heavy and light fluids with a heavy-fluid protrusion. Middle: the shock is transmitted through the interface, compressing the protrusion and setting the interface into motion, while a rarefaction is reflected. Bottom: the protrusion inverts and ejects a vortex ring into the heavy fluid.

heavy fluid of depth $L' = (\rho_H/\rho_{H^*})L$, starts inverting due to the sign of the vorticity. During inversion, the fluid in the protrusion is ejected into the heavy fluid at speed U_i relative to the interface, analogous to the piston speed in the classical system, entraining the light fluid and forming a vortex ring of density ρ_R . As in past studies [56], we model the ring as belonging to the Norbury [73] family, but must account for compressibility and multiple fluids. For an unsaturated ring, the circulation, impulse, and energy of the fluid slug ejected from the protrusion equal those corresponding to the ring. Extending the analysis to the present multi-material system yields:

$$\Gamma_{slug} = \frac{1}{2}L'U_i = \frac{1}{2}\frac{\rho_H}{\rho_{H^*}}LU_i = (\Omega\alpha l)\Gamma_N = \Gamma_{VR}, \quad (1a)$$

$$I_{slug} = \frac{1}{4}\rho_H\pi D^2LU_i = \rho_R(\Omega\alpha l)l^3I_N = I_{VR}, \quad (1b)$$

$$E_{slug} = \frac{1}{8}\rho_H\pi D^2LU_i^2 = \rho_R(\Omega\alpha l)^2l^3E_N = E_{VR}, \quad (1c)$$

where Ω is the vorticity density (i.e., vorticity divided by distance from the ring centerline [73]), α is the nondimensional mean vortex core radius, l is the ring radius, and the subscript N denotes nondimensional quantities that are functions only of α . Equations 1 can be rearranged to yield the formation number

$$\frac{L}{D} = \sigma\sqrt{\frac{\pi}{2}}\frac{I_N^{1/2}\Gamma_N^{3/2}}{E_N} = \sigma\sqrt{\frac{\pi}{2}}\frac{\Gamma_N^{3/2}}{U_N I_N^{1/2}}, \quad (2)$$

where $L' = \frac{\rho_H}{\rho_{H^*}}L$, $U_i = 2(\Omega\alpha l)U_N$ [56], and

$$\sigma = \sqrt{\frac{\rho_{H^*}\rho_H}{\rho_R\rho_H}}. \quad (3)$$

As with classical vortex rings, the formation number depends on the circulation, impulse, and energy, but now also depends on the shock strength and interface density

ratio. Equation 2 states that maximal circulation, impulse, and energy generated by the inverting protrusion is contained within the resulting ring. The parameter σ is a formation number multiplier generalizing the classical formation number (compare Equation 2 in the present work to Equations 12 and 13 in [56]) to rings generated from shocked interfaces, i.e.,

$$(L/D)_{sat, shock} = \sigma(L/D)_{sat, classical}. \quad (4)$$

The formation number multiplier accounts for both the interface density ratio and shock strength. The *multifluid factor* $\sqrt{\rho_{H^*}/\rho_R}$ is the square root of the relative density of the protrusion with respect to the ring after shock interaction. We approximate the ring density as the average of the post-shock fluid densities, $\rho_R \approx (\rho_{H^*} + \rho_{L^*})/2$, which is consistent with both simulations and the entrainment properties of saturated Norbury rings [73], though other mixing models could be used. As the density ratio is increased, the relative density of the vortex ring decreases. The resulting decrease in the ring's impulse and energy allows it to support additional impulse and energy from the inverting protrusion, which can be increased by increasing the protrusion depth (Equations 1b and 1c), thereby producing a larger formation number. The *compression factor* ρ_{H^*}/ρ_H describes shock compression of the protrusion. Because the circulation supplied by the inverting protrusion is proportional to protrusion depth and thus inversely proportional to shock strength (Equation 1a), the unshocked depth, and therefore formation number, must increase as the shock strength is increased to supply the same amount of circulation. If a vortex ring is produced with no compression ($\rho_{H^*} \rightarrow \rho_H$) and no density difference ($\rho_H \rightarrow \rho_L$), the classical limit $\sigma = 1$ is recovered. The classical formation number is generally accepted to be $3.0 \leq (L/D)_{sat} \leq 4.6$ [56], and therefore it is expected that in the present shock-accelerated case the formation number falls within the range

$$3.0\sigma \leq (L/D)_{sat, shock} \leq 4.6\sigma. \quad (5)$$

To verify these theoretical results, we use an in-house code [74–76] (see supplemental material [72]) solving the three-dimensional Euler equations for the setup in Figure 2. Sets of simulations, detailed in Table I, are performed for different density ratios and shock strengths similar to those in [21, 28, 29, 31, 47]. In cases 1-4, L is varied from 1 to 8 while keeping D constant. Cases 5 and 6 explore stronger shocks and larger interface density ratios. The simulations evolve in time long enough for pinch-off to occur, leading to a steady, self-propagating vortex ring identified by the $\lambda_2 = 0$ criterion, a standard method for identifying vortices based on eigenvalues, $\lambda_1 < \lambda_2 < \lambda_3$, related to the velocity gradient tensor [77]. To illustrate the dynamics, Figure 3 shows out-of-plane vorticity ω and density contours along the centerplane, as well as the three-dimensional surface of $\lambda_2 = 0$, for a shock of strength $\rho_{H^*}/\rho_H = 1.34$ with interface density ratio

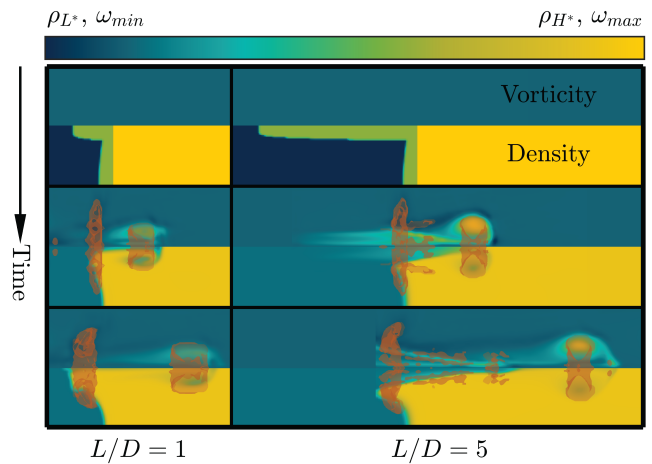


FIG. 3. Evolution of the vorticity (top) and density (bottom) following the interaction of a shock of strength $\rho_{H^*}/\rho_H = 1.34$ with heavy-fluid protrusions with aspect ratios $L/D = 1$ (left) and $L/D = 5$ (right) along an interface with $\rho_H/\rho_L = 2$. Orange surfaces enclose vortex rings, as identified by the $\lambda_2 = 0$ criterion [77].

$\rho_H/\rho_L = 2$ and protrusions of aspect ratios $L/D = 1$ and 5. For the $L/D = 1$ case, the protrusion inversion ejects a vortex ring that quickly pinches off and steadily separates from the original interface. Although some vorticity is confined to the interface, most of the vorticity is concentrated within the ring; there are no vortices between the ring and the interface. For the $L/D = 5$ case, which is near the formation number predicted by our theory, a pinched-off ring still steadily propagates away from the interface, but a trailing jet with vortices is evident. A known signature of exceeding the formation number, this jet forms because the saturated ring cannot support additional circulation from the vortex ring generator, which accumulates in the trailing jet [55].

These results suggest that the ring circulation saturates at sufficiently large protrusion aspect ratios, consistent with the classical case. To confirm that the formation number has been reached, Figure 4 shows the circulation of the pinched-off rings for different protrusion aspect ratios L/D . At low aspect ratios, the circulation of the ejected rings increases as the protrusion aspect ratio is increased. As L/D is further increased, however, the circulation saturates; at this point, no further circulation can be imparted to the ring. We take the formation number to be the value of L/D at the intersection of a line fit to points with $L/D \leq 3$, where the ring circulation appears to be growing linearly, and the average circulation of points with $L/D \geq 7$, where the circulation plateaus. The formation number for each set of simulations and the expected range based on our theory, summarized in Table I and the upper-left inset of Figure 4, differs from classical theory, but falls near the center of the range predicted by our extended theory.

As an example application, we estimate the formation number for the fill-tube jet for experiment N210808 at

the National Ignition Facility [4, 78] as

$$(L/D)_{sat,shock} = 3.8\sigma = 3.8\sqrt{\frac{2\rho_{e^*}}{\rho_{a^*} + \rho_{e^*}} \frac{\rho_{e^*}}{\rho_e}} \approx 7, \quad (6)$$

where ρ_{e^*} and ρ_{a^*} are the densities of the epoxy and ablator, respectively, after a strong shock releases off the ablator-ice interface and ρ_e is the unshocked epoxy density. Although a $2\mu\text{m}$ fill tube was utilized, the diameter of the epoxy-filled bore hole was $D = 8.4\mu\text{m}$ [78], making epoxy the appropriate material to model the protrusion. In this experiment, the ablator thickness was $L = 79\mu\text{m}$, and therefore $L/D = 9.4$. Because $L/D > (L/D)_{sat,shock}$, a saturated vortex ring and a trailing jet are expected, consistent with Figure 1. The circulation, impulse, and energy injected into the hotspot by the ring can then be calculated from Equation 1 with $L/D = (L/D)_{sat,shock}$. Furthermore, by replacing L with an integrated protrusion, or jet, velocity, our theory provides the timescale on which the ring forms. Although the calculated formation number appears to agree with observations of fill-tube jetting, the authors advise caution for direct applications to ICF, which involves fill-tube configurations that differ from our canonical setup, intense radiation, and convergent geometries. These and other effects would likely need to be considered for a precise determination of the fill-tube formation number.

The lack of a trailing jet for rings generated from smaller defects, and in the late nonlinear phase of the RMI, suggest that these rings are unsaturated. Both saturated and unsaturated rings transport kinetic energy, thus giving rise to a reduction in the kinetic energy of the mixing region the ring originates from. Ejected rings could also interact with other flow structures away from the mixing region. While the effects of viscosity and magnetic fields are not presently considered based on Reynolds number and plasma beta, Re and β , respectively, in ICF, where $Re \sim 10^4$ [79] and $\beta \sim 10^5$ [80], and for many supernovae, where $Re \sim 10^{10}$ and $\beta \sim 10^4$ [81], the conservation arguments central to our theory support a path to explore diffusive effects and magnetic fields. Because such mechanisms would tend to inhibit the conversion of circulation, impulse, and energy from the inverting protrusion to the vortex ring, a greater protrusion aspect ratio would likely be required to form a saturated ring. These and other effects, including molec-

TABLE I. Simulation parameters and expected formation numbers and ranges predicted by our theory.

Case	$\rho_{H'}/\rho_H$	M	ρ_H/ρ_L	3.0σ	4.6σ	$(L/D)_{sat,shock}$
1	1.17	1.1	2	3.94	6.05	5.16
2	1.17	1.1	5	4.27	6.54	5.52
3	1.34	1.2	2	4.42	6.78	5.47
4	1.34	1.2	5	4.65	7.13	6.03
5	1.86	1.5	8	5.54	8.50	6.79
6	2.67	2.0	11	6.33	9.70	7.59

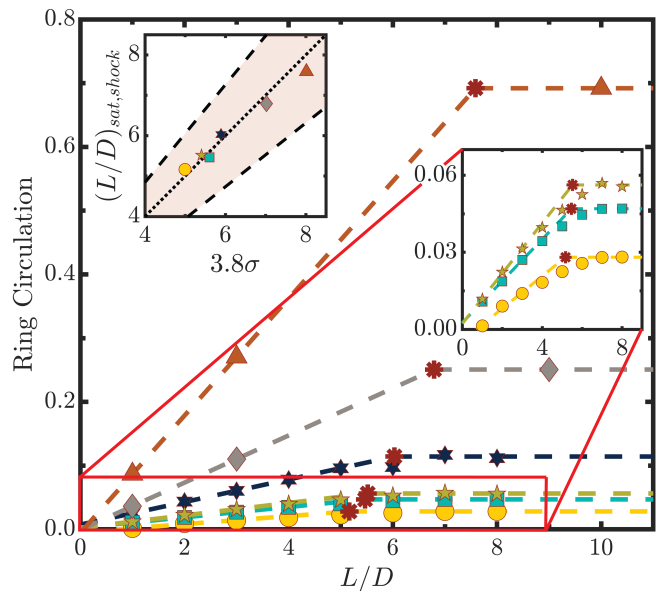


FIG. 4. Ring circulation vs. protrusion aspect ratio for cases 1-6 (yellow circles, green pentagrams, teal squares, dark blue hexagrams, grey diamonds, and orange triangles, respectively) in Table I. The right inset is a close-up of cases 1-3. The horizontal location of each red star identifies the formation number. The upper-left inset shows the formation number from simulations vs. our theory. The dotted line indicates where $(L/D)_{sat,shock} = 3.8\sigma$, and the dashed lines bound the shaded region where $3.0\sigma \leq (L/D)_{sat,shock} \leq 4.6\sigma$.

ular diffusion and radiation, may be quantifiable with appropriate source terms in Equation 1.

In this letter, we demonstrate that vortex rings generated following the interaction of a shock with a cylindrical protrusion originate due to the baroclinic torque deposited along the interface, which ejects the fluid initially in the protrusion as it inverts. The resulting dynamics are consistent with classical piston/cylinder systems, exhibiting ring saturation coincident with the emergence of a trailing jet. However, the formation number is augmented by a factor accounting for the different fluid densities and shock compression. Our analysis thus generalizes the classical theory to compressible multifluid flows and explains morphological differences observed in practice. While the computations presented support the theory, simulations exploring a wider range of parameters may help elucidate certain details, including late-time shock-induced turbulent mixing, as ejected vortex rings may affect mixing layer development and turbulent transition.

The present findings may have implications in ICF and astrophysics. In ICF, the fill tube may generate a vortex ring that impinges on the hotspot. Our theory also describes a mechanism that may affect mixing following supernovae and explain the presence of stellar core elements in the outer layers of expanding remnants. Furthermore, the results of our analysis could be used to deduce quantities of interest for shock-induced ejecta or

jets.

ACKNOWLEDGMENTS

This work is supported by the Lawrence Livermore National Laboratory under Subcontract No. B632749 and

the U. S. Department of Energy (DOE) as part of the Stewardship Science Graduate Fellowship Program under Grant No. De-NA0003960. Computational resources were provided by the Extreme Science and Engineering Discovery Environment Comet GPU system, USA under grant TG-CTS130005 and the Oak Ridge Leadership Computing Facility, a DOE Office of Science User Facility supported under Contract DE-AC05-00OR22725.

-
- [1] R. Betti and O. Hurricane, Inertial confinement fusion with lasers, *Nat. Phys.* **12**, 435 (2016).
- [2] A. B. Zylstra, A. L. Kritcher, O. A. Hurricane, D. A. Callahan, K. Baker, T. Braun, *et al.*, Record energetics for an inertial fusion implosion at NIF, *Phys. Rev. Lett.* **126**, 025001 (2021).
- [3] A. Zylstra, O. A. Hurricane, D. A. Callahan, A. L. Kritcher, J. E. Ralph, H. F. Robey, *et al.*, Burning plasma achieved in inertial fusion, *Nature* **601**, 542 (2022).
- [4] A. B. Zylstra, A. L. Kritcher, *et al.*, (Indirect Drive ICF Collaboration), Lawson criterion for ignition exceeded in an inertial fusion experiment, *Phys. Rev. Lett.* **129**, 075001 (2022).
- [5] G. R. Bennett, M. C. Herrmann, M. J. Edwards, B. K. Spears, C. A. Back, E. W. Breden, *et al.*, Fill-tube-induced mass perturbations on x-ray-driven, ignition-scale, inertial-confinement-fusion capsule shells and the implications for ignition experiments, *Phys. Rev. Lett.* **99**, 205003 (2007).
- [6] M. J. Schmitt, P. A. Bradley, J. A. Cobble, J. R. Fincke, P. Hakel, S. C. Hsu, *et al.*, Development of a polar direct-drive platform for studying inertial confinement fusion implosion mix on the National Ignition Facility, *Phys. Plasmas* **20**, 056310 (2013).
- [7] I. V. Igumenshchev, N. V. Goncharov, W. T. Shmayda, D. R. Harding, T. C. Sangster, and D. D. Meyerhofer, Effects of local defect growth in direct-drive cryogenic implosions on OMEGA, *Phys. Plasmas* **20**, 082703 (2013).
- [8] S. P. Regan, R. Epstein, B. A. Hammel, L. J. Suter, H. A. Scott, M. A. Barrios, *et al.*, Hot-spot mix in ignition-scale inertial confinement fusion targets, *Phys. Rev. Lett.* **111**, 045001 (2013).
- [9] C. R. Weber, T. Döppner, D. T. Casey, T. L. Bunn, L. C. Carlson, R. J. Dylla-Spears, *et al.*, First measurements of fuel-ablator interface instability growth in inertial confinement fusion implosions on the National Ignition Facility, *Phys. Rev. Lett.* **117**, 075002 (2016).
- [10] B. M. Haines, R. E. Olson, W. Sweet, S. A. Yi, A. B. Zylstra, P. A. Bradley, *et al.*, Robustness to hydrodynamic instabilities in indirectly driven layered capsule implosions, *Phys. Plasmas* **26**, 012707 (2019).
- [11] A. B. Zylstra, D. T. Casey, A. Kritcher, L. Pickworth, B. Bachmann, K. Baker, *et al.*, Hot-spot mix in large-scale HDC implosions at NIF, *Phys. Plasmas* **27**, 092709 (2020).
- [12] S. I. Abarzhi, A. K. Bhowmick, A. Naveh, A. Pandian, N. C. Swisher, R. F. Stellingwerf, and W. D. Arnett, Supernova, nuclear synthesis, fluid instabilities, and interfacial mixing, *Proc. Natl. Acad. Sci. U.S.A.* **116**, 18184 (2019).
- [13] J. Kane, R. P. Drake, and B. A. Remington, An evaluation of the Richtmyer-Meshkov instability in supernova remnant formation, *Astrophys. J.* **511**, 335 (1999).
- [14] C. C. Kuranz, R. P. Drake, M. J. Grasskopf, A. Budde, C. Krauland, D. C. Marion, *et al.*, Three-dimensional blast-wave-driven Rayleigh-Taylor instability and the effects of long-wavelength modes, *Phys. Plasmas* **16**, 056310 (2009).
- [15] C. C. Kuranz, R. P. Drake, E. C. Harding, M. J. Grasskopf, H. F. Robey, B. A. Remington, *et al.*, Two-dimensional blast-wave-driven Rayleigh-Taylor instability: experiment and simulation, *Astrophys. J.* **696**, 749 (2009).
- [16] N. J. Zabusky, Are cosmic knots escaped vortex projectiles?, *APS April Meeting Abstracts*, K12 (1997).
- [17] A. Banerjee, R. A. Gore, and M. J. Andrews, Development and validation of a turbulent-mix model for variable-density and compressible flows, *Phys. Rev. E* **82**, 046309 (2010).
- [18] G. Dimonte and R. Tipton, K-L turbulence model for the self-similar growth of the Rayleigh-Taylor and Richtmyer-Meshkov instabilities, *Phys. Fluids* **18**, 085101 (2006).
- [19] R. D. Richtmyer, Taylor instability in shock-acceleration of compressible fluids, *Comm. Pure Appl. Math* **8**, LA-1914 (del.) (1960).
- [20] E. E. Meshkov, Instability of the interface of two gases accelerated by a shock wave, *Fluid Dyn.* **4**, 101 (1969).
- [21] B. D. Collins and J. W. Jacobs, PLIF flow visualization and measurements of the Richtmyer-Meshkov instability of an air/SF₆ interface, *J. Fluid Mech.* **464**, 113 (2002).
- [22] O. Sadot, L. Erez, U. Alon, D. Oron, L. A. Levin, G. Erez, G. Ben-Dor, and D. Shvarts, Study of the nonlinear evolution of single-mode and two-bubble interaction under Richtmyer-Meshkov instability, *Phys. Rev. Lett.* **80**, 1654 (1998).
- [23] J. W. Jacobs and J. M. Sheeley, Experimental study of incompressible Richtmyer-Meshkov instability, *Phys. Fluids* **8**, 405 (1995).
- [24] A. Rikanati, U. Alon, and D. Shvarts, Vortex model for the nonlinear evolution of the multimode Richtmyer-Meshkov instability at low Atwood numbers, *Phys. Rev. E* **58**, 7410 (1998).
- [25] O. A. Likhachev and J. W. Jacobs, A vortex model for Richtmyer-Meshkov instability accounting for finite Atwood number, *Phys. Fluids* **17**, 031704 (2005).
- [26] S. Pellone, C. A. Di Stefano, A. M. Rasmus, C. C. Kuranz, and E. Johnsen, Vortex-sheet modeling of hydrodynamic instabilities produced by an oblique shock interacting with a perturbed interface in the HED regime, *Phys. Plasmas* **28**, 022303 (2021).

- [27] M. Latini, O. Schilling, and W. S. Don, Effects of WENO flux reconstruction order and spatial resolution on reshocked two-dimensional Richtmyer-Meshkov instability, *J. Comput. Phys.* **221**, 805 (2007).
- [28] E. G. Sewell, K. J. Ferguson, V. V. Krivets, and J. W. Jacobs, Time-resolved particle image velocimetry measurements of the turbulent Richtmyer-Meshkov instability, *J. Fluid Mech.* **917** (2021).
- [29] B. J. Olson and J. A. Greenough, Comparison of two- and three-dimensional simulations of miscible Richtmyer-Meshkov instability with multimodal initial conditions, *Phys. Fluids* **26**, 101702 (2014).
- [30] I. W. Kokkinakis, D. Drikakis, and D. L. Youngs, Vortex morphology in Richtmyer-Meshkov-induced turbulent mixing, *Physica D* **407**, 132459 (2020).
- [31] R. H. Cohen, W. P. Dannevik, A. M. Dimits, D. E. Eliaison, A. A. Mirin, Y. Zhou, D. H. Porter, and P. R. Woodward, Three-dimensional simulation of a Richtmyer-Meshkov instability with a two-scale initial perturbation, *Phys. Fluids* **14**, 3692 (2002).
- [32] P. Movahed and E. Johnsen, A solution-adaptive method for efficient compressible multifluid simulations, with application to the Richtmyer-Meshkov instability, *J. Comput. Phys.* **239**, 166 (2013).
- [33] D. Tordella and M. Iovieno, Small-scale anisotropy in turbulent shearless mixing, *Phys. Rev. Lett.* **107**, 194501 (2011).
- [34] D. Layzer, On the instability of superposed fluids in a gravitational field, *Astrophys. J.* **122**, 1 (1955).
- [35] A. L. Velikovich, Nonlinear perturbation theory of the incompressible Richtmyer-Meshkov instability, *Phys. Rev. Lett.* **76**, 3112 (1996).
- [36] R. L. Holmes, G. Dimonte, B. Fryxell, M. L. Gittings, J. W. Grove, M. Schneider, D. H. Sharp, A. L. Velikovich, F. P. Weaver, and Q. Zhang, Richtmyer-Meshkov instability growth: experiment, simulation and theory, *J. Fluid Mech.* **389**, 55 (1999).
- [37] Y. Zhou, Rayleigh-Taylor and Richtmyer-Meshkov instability induced flow, turbulence, and mixing. I, *Phys. Rep.* **720-722**, 1 (2017).
- [38] Y. Zhou, Rayleigh-Taylor and Richtmyer-Meshkov instability induced flow, turbulence, and mixing. II, *Phys. Rep.* **723-725**, 1 (2017).
- [39] A. Y. Faenov, T. A. Pikuz, P. Mabey, B. Albertazzi, T. Michel, G. Rigon, *et al.*, Advanced high resolution x-ray diagnostic for HEDP experiments, *Sci. Rep.* **8**, 1 (2018).
- [40] A. Do, A. M. Angulo, G. N. Hall, S. R. Nagel, N. Izumi, B. J. Kozioziemski, T. McCarville, J. M. Ayers, and D. K. Bradley, X-ray imaging of Rayleigh-Taylor instabilities using Fresnel zone plate at the National Ignition Facility, *Rev. Sci. Instrum.* **92**, 053511 (2021).
- [41] F. J. Marshall, S. T. Ivancic, C. Mileham, P. M. Nilson, J. J. Ruby, C. Stoeckl, B. S. Scheiner, and M. J. Schmitt, High-resolution x-ray radiography with Fresnel zone plates on the University of Rochester's OMEGA laser systems, *Rev. Sci. Instrum.* **92**, 033701 (2021).
- [42] G. Rigon, B. Albertazzi, T. Pikuz, P. Mabey, V. Bouffetier, N. Ozaki, *et al.*, Micron-scale phenomena observed in a turbulent laser-produced plasma, *Nat. Commun.* **12**, 1 (2021).
- [43] B. Thornber and Y. Zhou, Numerical simulations of the two-dimensional multimode Richtmyer-Meshkov instability, *Phys. Plasmas* **22**, 032309 (2015).
- [44] S. Balasubramanian, G. C. Orlicz, and K. P. Prestridge, Experimental study of initial condition dependence on turbulent mixing in shock-accelerated Richtmyer-Meshkov fluid layers, *J. Turbul.* **14**, 170 (2013).
- [45] K. L. Baker, C. A. Thomas, T. R. Dittrich, O. Landen, G. Kyrala, D. T. Casey, *et al.*, Fill tube dynamics in inertial confinement fusion implosions with high density carbon ablaters, *Phys. Plasmas* **27**, 112706 (2020).
- [46] B. A. Hammel, H. A. Scott, S. P. Regan, C. Cerjan, D. S. Clark, M. J. Edwards, *et al.*, Diagnosing and controlling mix in National Ignition Facility implosion experiments, *Phys. Plasmas* **18**, 056310 (2011).
- [47] M. Wadas and E. Johnsen, Interactions of two bubbles along a gaseous interface undergoing the Richtmyer-Meshkov instability in two dimensions, *Physica D* **409**, 132489 (2020).
- [48] B. Thornber and Y. Zhou, Energy transfer in the Richtmyer-Meshkov instability, *Phys. Rev. E* **86**, 056302 (2012).
- [49] Y. Zhou, M. Groom, and B. Thornber, Dependence of enstrophy transport and mixed mass on dimensionality and initial conditions in the Richtmyer-Meshkov instability induced flows, *J. Fluids Enj.* **142**, 12 (2020).
- [50] N. J. Zabusky and S. Zhang, Shock-planar curtain interactions in two dimensions: emergence of vortex double layers, vortex projectiles, and decaying stratified turbulence, *Phys. Fluids* **14**, 419 (2002).
- [51] S. Zhang and N. J. Zabusky, Shock-planar curtain interactions: strong secondary baroclinic deposition and emergence of vortex projectiles and late-time inhomogeneous turbulence, *Laser Part. Beams* **21**, 463 (2003).
- [52] U. Alon, J. Hecht, D. Mukamel, and D. Shvarts, Scale invariant mixing rates of hydrodynamically unstable interfaces, *Phys. Rev. Lett.* **72**, 2867 (1994).
- [53] J. Hecht, U. Alon, and D. Shvarts, Potential flow models of Rayleigh-Taylor and Richtmyer-Meshkov bubble fronts, *Phys. Fluids* **6**, 4019 (1994).
- [54] K. O. Mikaelian, Analytic approach to nonlinear Rayleigh-Taylor and Richtmyer-Meshkov instabilities, *Phys. Rev. Lett.* **80**, 508 (1998).
- [55] M. Gharib, E. Rambod, and K. Shariff, A universal time scale for vortex ring formation, *J. Fluid Mech.* **360**, 121 (1998).
- [56] K. Mohseni and M. Gharib, A model for universal time scale of vortex ring formation, *Phys. Fluids* **10**, 2436 (1998).
- [57] P. A. Keiter, J. Elliott, B. Blue, J. Cooley, J. Edwards, G. Kyrala, H. Robey, B. Spears, and D. Wilson, Measurement and simulation of jet mass caused by a high-aspect ratio hole perturbation, *Phys. Plasmas* **17**, 062704 (2010).
- [58] B. E. Blue, H. F. Robey, S. G. Glendinning, M. J. Bono, S. C. Burkhart, J. R. Celeste, *et al.*, Three-dimensional hydrodynamic experiments on the National Ignition Facility, *Phys. Plasmas* **12**, 056313 (2005).
- [59] P. Hartigan, J. Foster, B. Wilde, R. Coker, P. Rosen, J. Hansen, B. Blue, R. Williams, R. Carver, and A. Frank, Laboratory experiments, numerical simulations, and astronomical observations of deflected supersonic jets: application to HH 110, *Astrophys. J.* **705**, 1073 (2009).
- [60] W. T. Buttler, D. M. Oró, D. L. Preston, K. O. Mikaelian, F. J. Cherne, R. S. Hixson, *et al.*, Unstable Richtmyer-Meshkov growth of solid and

- liquid metals in vacuum, *J. Fluid Mech.* **703**, 60 (2012).
- [61] A. M. Saunders, C. V. Stan, K. K. Mackay, B. Morgan, J. A. K. Horwitz, S. J. Ali, *et al.*, Experimental observations of laser-driven tin ejecta microjet interactions, *Phys. Rev. Lett.* **127**, 155002 (2021).
- [62] T. Maxworthy, Some experimental studies of vortex rings, *J. Fluid Mech.* **81**, 465 (1977).
- [63] M. Nitsche and R. Krasney, A numerical study of vortex ring formation at the edge of a circular tube, *J. Fluid Mech.* **276**, 139 (1994).
- [64] S. C. Shadden, K. Katija, M. Rosenfeld, J. E. Marsden, and J. O. Dabiri, Transport and stirring induced by vortex formation, *J. Fluid Mech.* **593**, 315 (2007).
- [65] M. Rosenfeld, E. Rambod, and M. Gharib, Circulation and formation number of laminar vortex rings, *J. Fluid Mech.* **376**, 297 (1998).
- [66] K. Mohseni, H. Ran, and T. Colonius, Numerical experiments on vortex ring formation, *J. Fluid Mech.* **430**, 267 (2001).
- [67] J. O. Dabiri and M. Gharib, Fluid entrainment by isolated vortex rings, *J. Fluid Mech.* **511**, 311 (2004).
- [68] G. Pawlak, C. M. Cruz, C. M. Bazán, and P. G. Hrdy, Experimental characterization of starting jet dynamics, *Fluid Dyn. Res.* **39**, 711 (2007).
- [69] R. Sau and K. Mahesh, Passive scalar mixing in vortex rings, *J. Fluid Mech.* **582**, 449 (2007).
- [70] M. Rosenfeld, K. Katija, and J. O. Dabiri, Circulation generation and vortex ring formation by conic nozzles, *J. Fluids Enj.* **131**, 9 (2009).
- [71] I. Danaila, F. Luddens, F. Kaplanski, A. Papoutsakis, and S. S. Sazhin, Formation number of confined vortex rings, *Phys. Rev. Fluids* **3**, 094701 (2018).
- [72] See Supplemental Material at [URL will be inserted by publisher] for a description of the protrusion inversion process, simulation numerical details, estimation of fill-tube formation number, and verification of theory for shocks of moderate strength.
- [73] J. Norbury, A family of steady vortex rings, *J. Fluid Mech.* **57**, 417 (1973).
- [74] M. Henry de Frahan, P. Movahed, and E. Johnsen, A new limiting procedure for discontinuous Galerkin methods applied to compressible multiphase flows with shocks and interfaces, *J. Comput. Phys.* **280**, 489 (2015).
- [75] P. Johnson and E. Johnsen, The compact gradient recovery discontinuous Galerkin method for diffusion problems, *J. Comput. Phys.* **398**, 108872 (2019).
- [76] M. Henry de Frahan, P. Movahed, and E. Johnsen, Numerical simulations of a shock interacting with successive interfaces using the discontinuous Galerkin method: the multilayered Richtmyer-Meshkov and Rayleigh-Taylor instabilities, *Shock Waves* **25**, 329 (2015).
- [77] J. Jeong and F. Hussain, On the identification of a vortex, *J. Fluid Mech.* **285**, 69 (1995).
- [78] J. Kuczek and B. Haines, The impact of fill tube geometry on recent high yield implosions on the National Ignition Facility, Talk presented at the 17th International Workshop on the Physics of Compressible Turbulent Mixing. (2022). https://drive.google.com/drive/folders/1CYPWJZ5DuZjRt7DgFC_VE10ez_oMChJ1?usp=share_link
- [79] C. R. Weber, D. S. Clark, A. W. Cook, L. E. Busby, and H. F. Robey, Inhibition of turbulence in inertial-confinement-fusion hot spots by viscous dissipation, *Phys. Rev. E* **89**, 053106 (2014).
- [80] B. Srinivasan, G. Dimonte, and X.-Z. Tang, Magnetic field generation in Rayleigh-Taylor unstable inertial confinement fusion plasmas, *Phys. Rev. Lett.* **108**, 165002 (2012).
- [81] D. Ryutov, R. P. Drake, J. Kane, E. Liang, B. A. Remington, and W. M. Wood-Vasey, Similarity criteria for the laboratory simulation of supernova hydrodynamics, *Astrophys. J.* **518**, 821 (1999).